Electronic Supplementary Material (ESI) for Journal of Materials Chemistry A.

Supporting Information

Highly Stretchable, Self-healable, Transparent and Solid-State Poly(Ionic Liquid) Filler for High-Performance Dielectric Elastomer Actuators

Hui Wang,[a] Matthew Wei Ming Tan,[a,b] Wei Church Poh,[a] Dace Gao,[a] Wenting Wu [a] and Pooi See Lee[a,b]*

[a] School of Materials Science and Engineering, Nanyang Technological University, 50 Nanyang Avenue, Singapore 639798, Singapore.
E-mail: pslee@ntu.edu.sg
[b] Singapore-HUJ Alliance for Research and Enterprise (SHARE), Smart Grippers for Soft Robotics (SGSR), Campus for Research Excellence and Technological Enterprise (CREATE), Singapore 138602, Singapore.

1. Methods

Materials

1-vinylimizadole (>98%), and 1-bromohexane (>98%) were purchased from TCI Chemicals. Poly(ethylene glycol) diacrylate (PEGDA700, M_n 700), diphenyl(2,4,6-trimethylbenzoyl)phosphine oxide (TPO, 97%), sodium tetrafluoroborate ($NaBF_4$) were purchased from Sigma-Aldrich. Carbon grease was procured from Nanjing Xilite Adhesive Co. Ltd. Commercial silver nanowire (AgNW) was purchased from Xfnano Technology with diameters of 50 nm and length of 100 ~ 200 mm. The AgNW solution in isopropyl alcohol (IPA) was diluted into a concentration of 0.5 mg/mL before use.

Characterization

^{1}H NMR spectrum was obtained from Bruker Avance DPX-400 (400 MHz) Fourier-transform NMR spectrometer at 298 K and calibrated against tetramethylsilane, $Si(CH_3)_4$. All FTIR spectra were collected in the wavenumber range of 4000-600 cm^{-1} by a PerkinElmer Fourier Transform Infrared (FTIR) Frontier spectrometer with attenuated total reflection (ATR) accessory, which average over 16 scans at a resolution of 1 cm^{-1}. TGA was done through ramping from room temperature to 700 ºC at 10 ºC min^{-1} to determine the thermal stability of PILs. DSC was applied to determine the T_g of different PILs by cooling/heating at 10 ºC min^{-1}. The transparency of PIL-100, VHB and C-VHB (composite VHB consists of VHB and PIL filler) was determined by absorption spectra using a Perkin Elmer Lambda 950 spectrophotometer in transmittance mode. The rheology of different PILs was measured by a MCR 702e (Anton Paar) rheometer using a plain-plate geometry (PP-10) in an oscillation mode at angular frequencies from 0.1 to 100 rad/s. For swelling tests, different PILs with an area of 1 × 1 cm^2 were placed in petri dishes respectively. Then they were immersed in acetonitrile and equilibrated at room temperature for 2 days. Swelling ratio Q is defined as the difference between the initial weight of dry PIL (M_0) and the weight at swelling equilibrium (M_s) divided by the initial weight the ratio of the weight to that in the as-prepared state, $Q = (M_s–M_0)/M_0$. Three independent samples were measured to calculate the standard deviation. Emission from the light emissive bending DEA was collected by an optical fiber connected to an Acton SP-2300 monochromator. Emission spectra from the light emissive bending DEA were measured by a Princeton Pixis 100B spectroscopy CCD detector on the monochromator. The capacitance and dielectric loss were measured simultaneously by a dielectric spectroscopy (Agilent 4294A). The dielectric constant of VHB and C-VHB was calculated by the equation $\varepsilon_r = \frac{C\,d}{\varepsilon_0 A}$, where C,

d, ε_0 and A are capacitance, thickness of the elastomer, vacuum dielectric constant and the area of electrodes, respectively. The thickness is controlled as the same of 250 μm, and the electrode area is the same as well. The dielectric breakdown strength of VHB and C-VHB was measured based on ASTM D3755-20. Samples were immersed in silicone oil to avoid the existence of oxygen and both sides of the samples were contacted with disk copper electrodes which connect to a high voltage power source. Ten samples of each type of elastomers were tested for Weibull analysis. The relationship between cumulative failure probability and breakdown field is described as $P(E) = 1 - e^{-(\frac{E}{E_b})^{\beta}}$, where E_b and β are dielectric breakdown field and Weibull modulus respectively.[1]

Mechanical Test

All the samples for mechanical tests were cut into rectangular shape with a length of ~20 mm, a width of ~10 mm. The thickness of independent PIL-100, VHB 4905, C-VHB is ~0.7, 0.5, ~1.25 mm, respectively. The stress–strain curves were obtained with MTS criterion model 42 (MTS Systems Corporation, Eden Prairie, MN, USA) static mechanical tester at a strain rate of 100 mm/min. Three independent samples for each PIL were measured to calculate the standard deviation. Young's modulus was obtained from the slopes of tensile curves from 0% to 5% strain.

Shear Test

The shear test was conducted by MTS criterion model 42 (MTS Systems Corporation, Eden Prairie, MN, USA) static mechanical tester according to ASTM D1002. VHB 4905 (or PDMS) and PIL-100 were fixed on two stainless steel plates respectively. Then the two materials were overlapped to make a contact. The length and width of the overlapping region are 12.7 and 21 mm, respectively. The gripper holding the steel with PIL-100 was pulling up with a speed of 1.3 mm/min while the VHB was fixed by the bottom gripper.

Probe Tack Test

A probe with a diameter of 12 mm was held by an upper gripper which was controlled by MTS criterion model 42 (MTS Systems Corporation, Eden Prairie, MN, USA) static mechanical tester. PILs were cured on the steel plates and fixed on the bottom plate below the probe. By moving the upper gripper, a good contact between probe and PILs was first established by pressing the probe onto PILs with a constant contact force of 5 N for 1 min. Subsequently, the

probe was pulled up with a constant separation speed of 0.01 mm/s. The force required for separation of the probe from the surface of PILs was recorded as a function of distance by the mechanical tester. The integral areas under the force-distance curves demonstrate the adhesion energy.

Calculation

For bending DEAs, specific energy density E_{mass} is calculated by the following equation:[2]

$$E_{mass} = \frac{F_b \alpha}{2m} \qquad (1)$$

where F_b, α, m are blocking force, bending displacement and mass of DEAs, respectively. Here, m for DEA with VHB and C-VHB (including electrodes and passive layers) are 0.1678 and 0.2782 g, respectively. Equation 2 can be used to transfer bending angles θ to bending displacements α with known length l of DEAs.

$$\alpha = \frac{\pi \theta l}{180} \qquad (2)$$

Here l for DEAs with VHB and C-VHB is the same, namely 23 mm.

Electromechanical conversion efficiency (σ) is the ratio of mechanical work output to electrical energy input, which can be calculated by:[3]

$$\sigma = \frac{E_{mechanical}}{E_{electrical}} = \frac{\alpha F_b/2}{CV^2/2} \qquad (3)$$

where C and V are capacitance and voltage, respectively.

2. Supplementary Figures and Tables

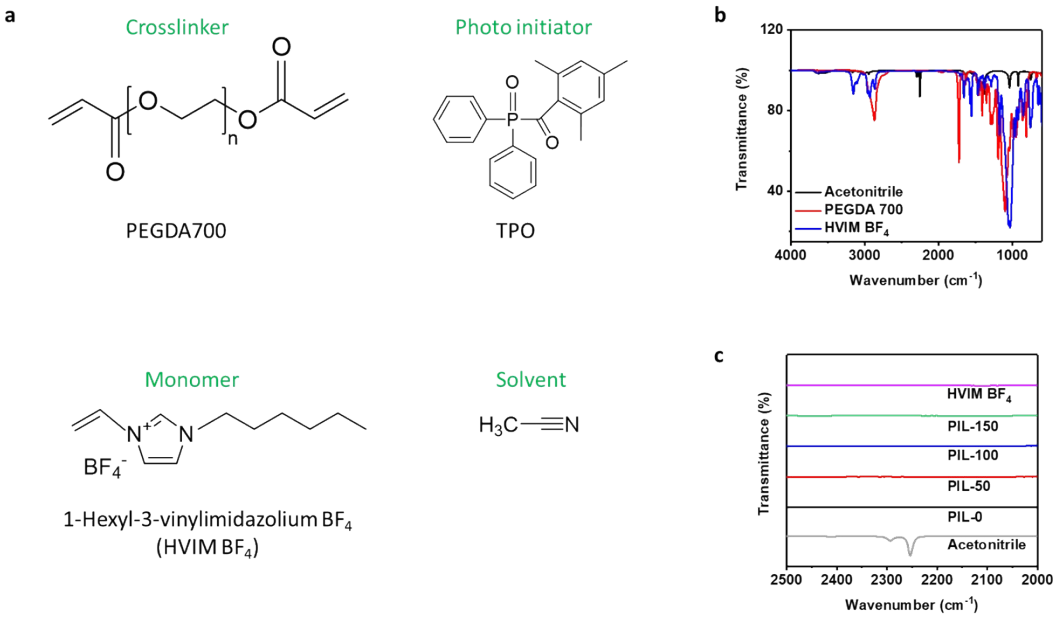

Fig. S1. (a) Molecular structure of raw materials of PILs. (b) FTIR spectra of raw materials of PILs. (c) FTIR spectra of HVIM BF_4, different PILs and acetonitrile.

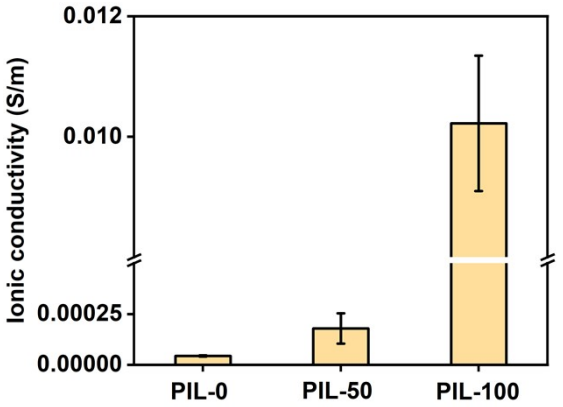

Fig. S2. Ionic conductivity of PIL-0, PIL-50, PIL-100 (error bars: standard deviations), which is 4.39×10^{-5}, 1.79×10^{-4}, 0.0102 S/m, respectively.

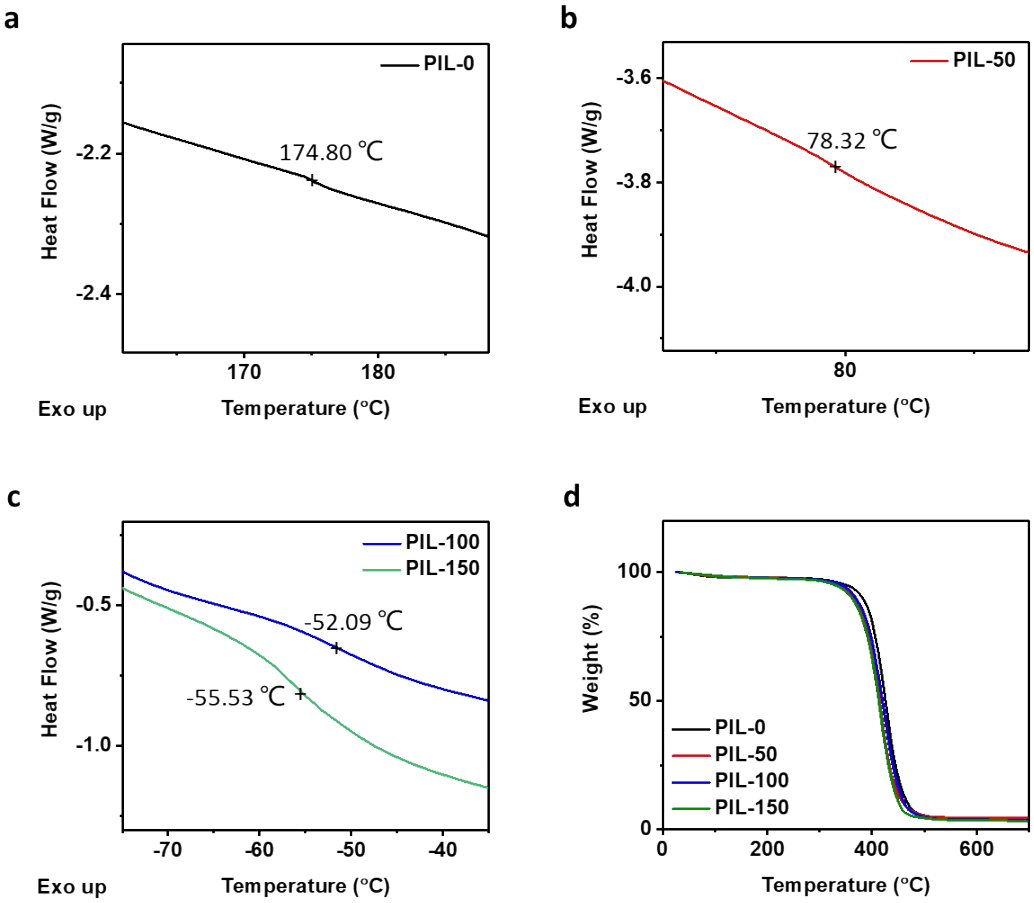

Fig. S3. (a, b, c) DSC thermograms of different PILs. (d) Thermogravimetric analysis (TGA) of different PILs.

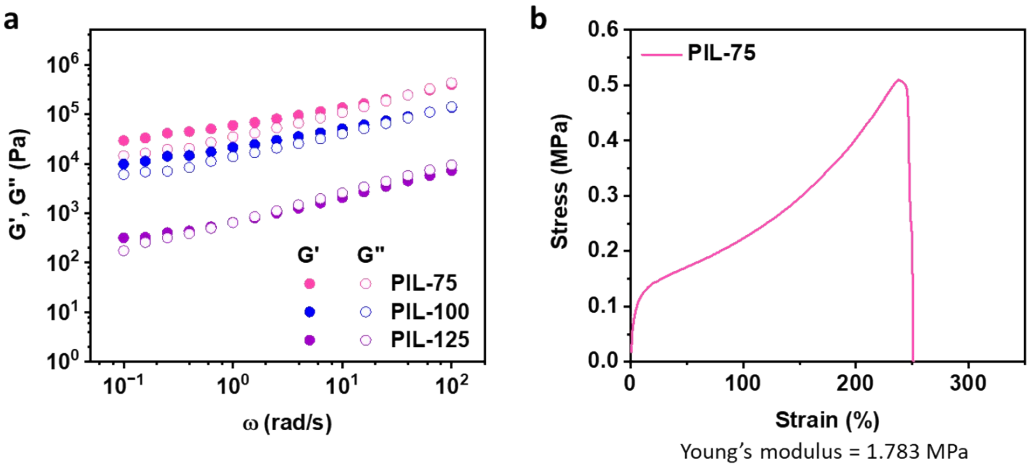

Fig. S4. (a) Frequency-dependent storage modulus (G') and loss modulus (G") of PIL-75, PIL-100 and PIL-125. PIL-125 is more liquid-like than PIL-100 while PIL-75 is more solid-like. (b) Tensile stress–strain curves of PIL-75 at a loading rate of 100 mm/min.

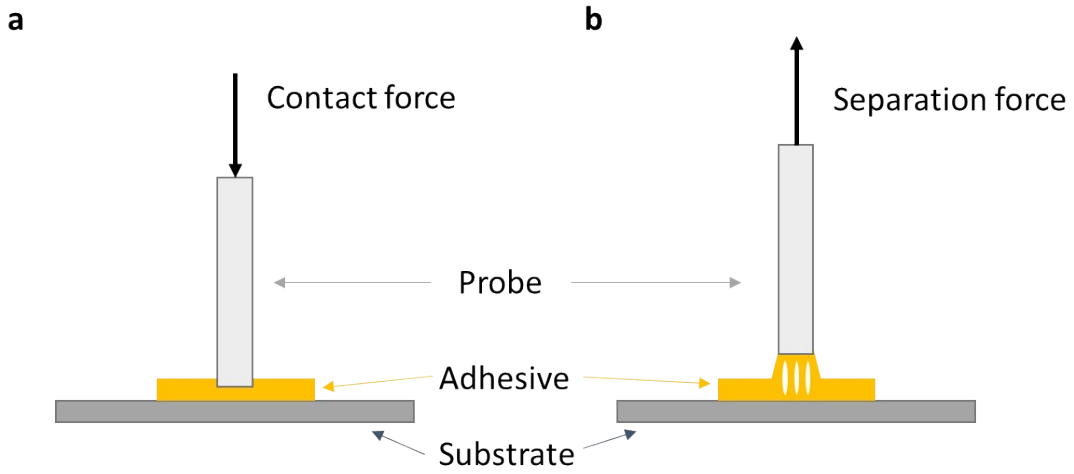

Fig. S5. Schematic representation of a typical tack adhesion measurement apparatus during contact and separation steps.

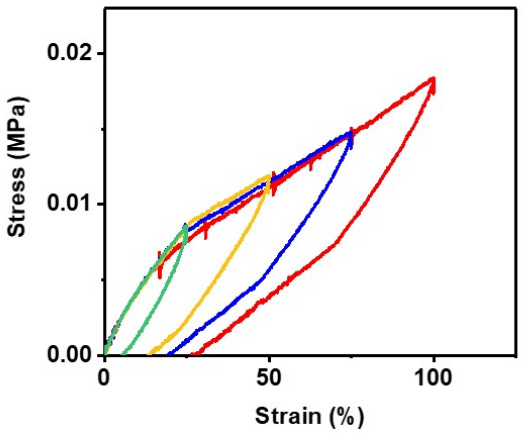

Fig. S6. Cyclic stress–strain curves of PIL-100 to various strains of 25%, 50%, 75% and 100%.

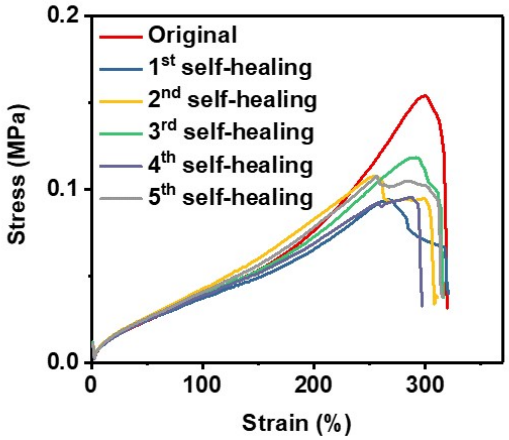

Fig. S7. Stress–strain curves of PIL-100 for 5 cycles of self-healing.

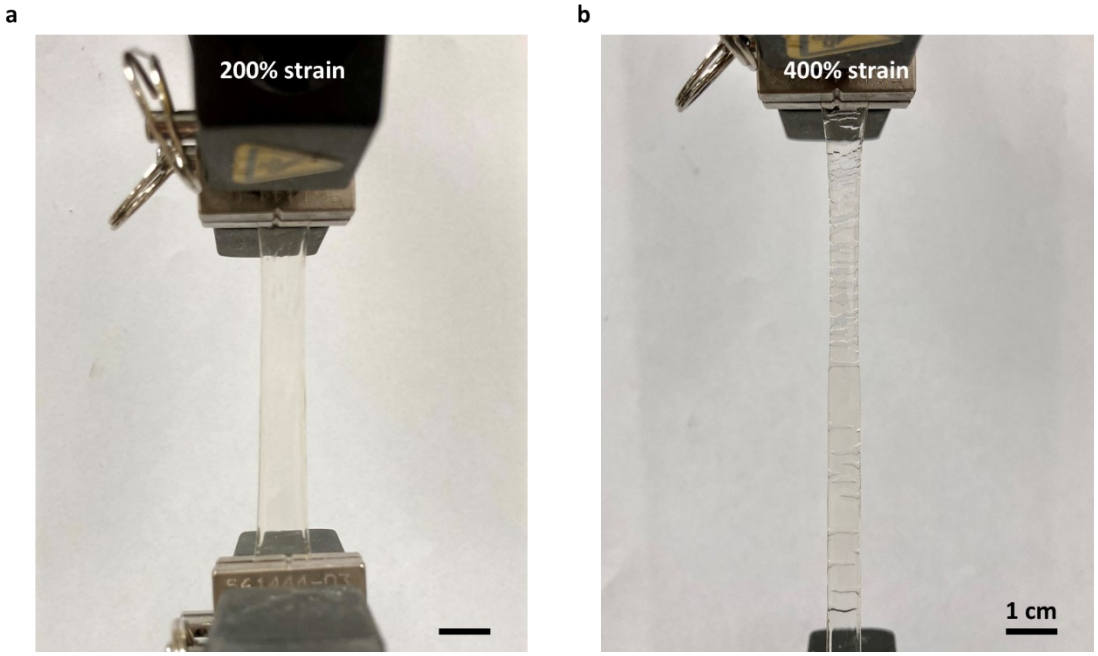

Fig. S8. (a) Photograph of C-VHB at 200% strain showing a great contact between VHB and PIL filler. (b) Photograph of C-VHB at 400% strain showing delamination.

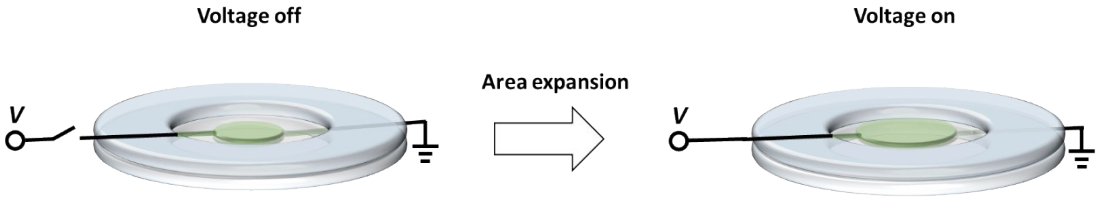

Fig. S9. Schematic representation of DEA with area strain.

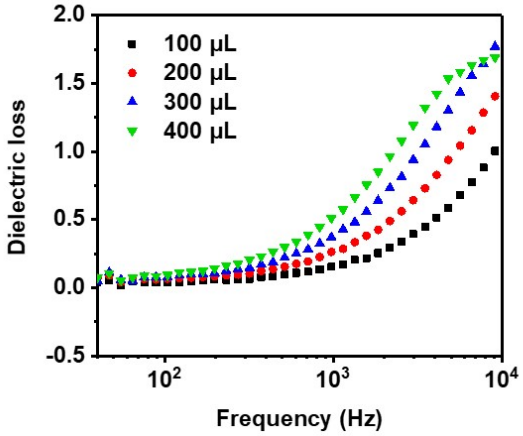

Fig. S10. Dielectric loss of C-VHB with different loadings of PIL precursor at different frequencies measured by dielectric spectroscopy.

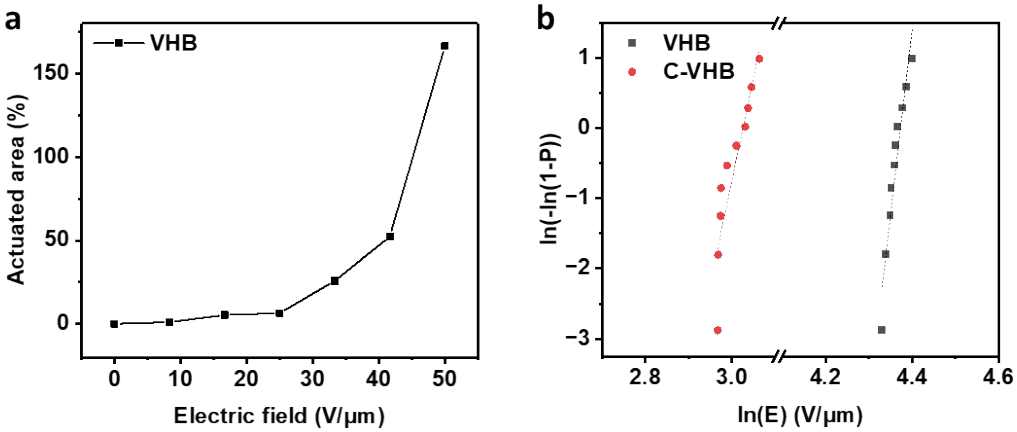

Fig. S11. (a) Actuated area of DEA with VHB. (b) Weibull distribution of dielectric breakdown strength of VHB and C-VHB.

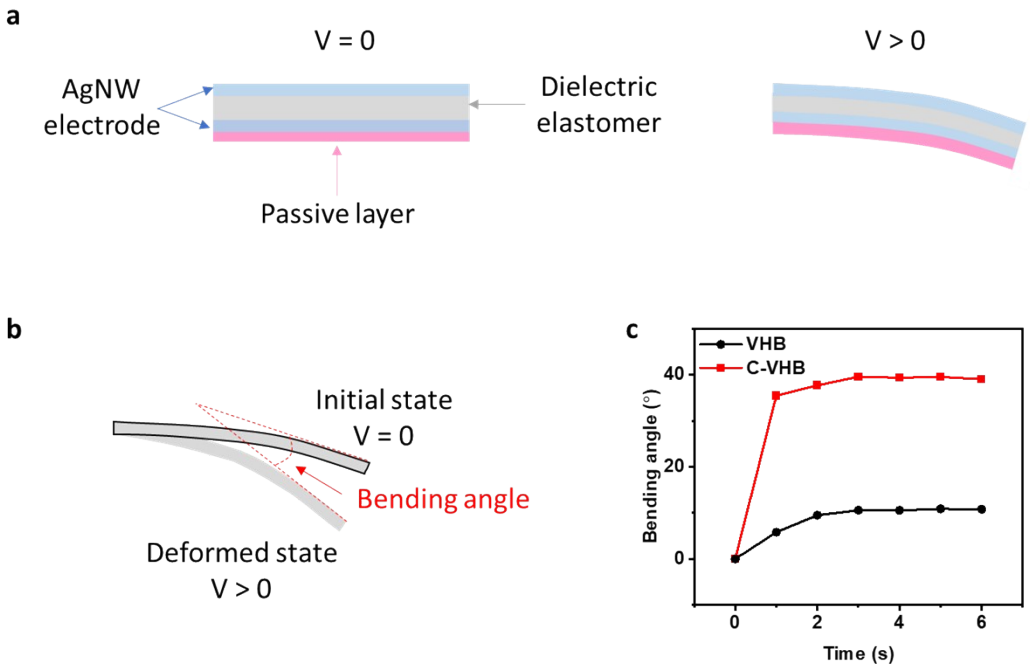

Fig. S12. (a) Schematic representation of bending DEAs in the off and on state. (b) Schematic representation of the measurement of bending angle. (c) Dependence of bending angle on time of voltage applied (12 V/μm for VHB, 12.6 V/μm for C-VHB), which shows equilibrium state after 3 seconds.

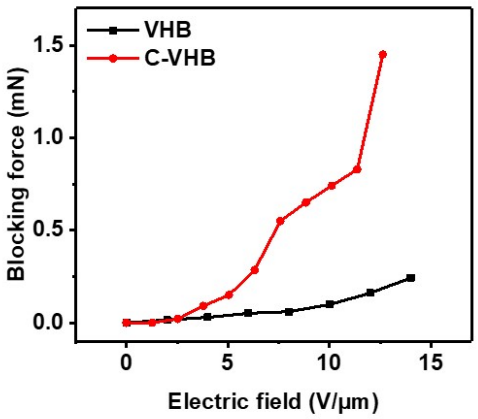

Fig. S13. Blocking forces of DEAs with VHB and C-VHB.

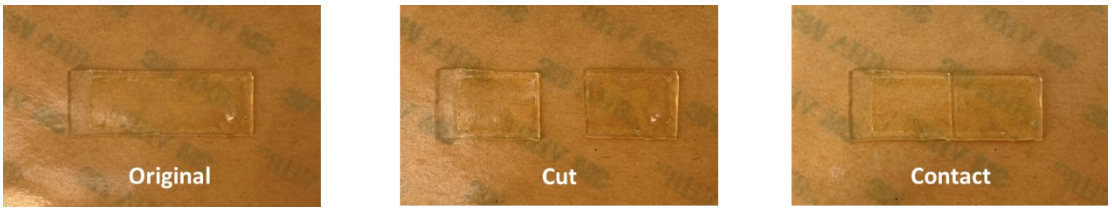

Fig. S14. The original, cut, contact state of C-VHB to illustrate the recoverability.

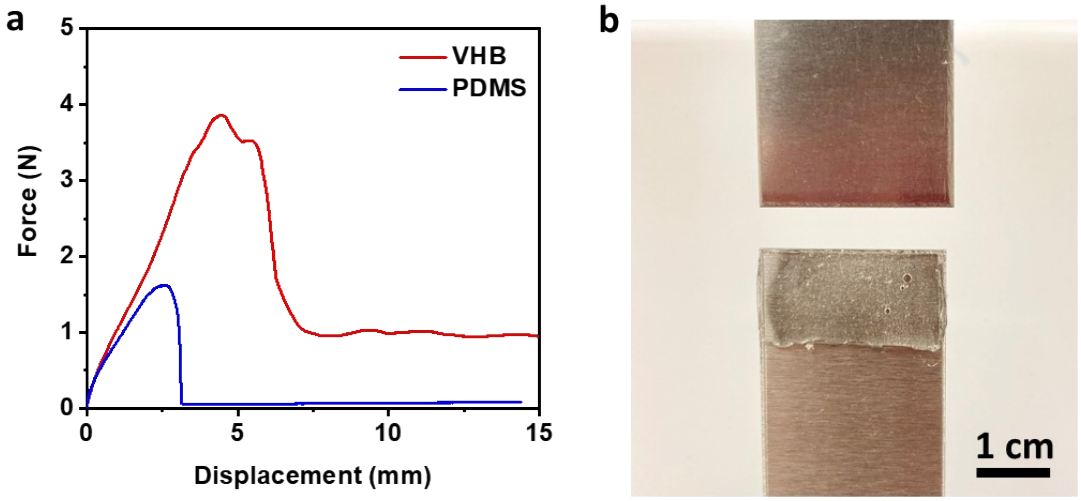

Fig. S15. (a) Adhesion forces between PIL-100 and VHB or PDMS, measured by shear tests. (b) Digital photograph of PIL-100 being pulled up showing no cohesive failure.

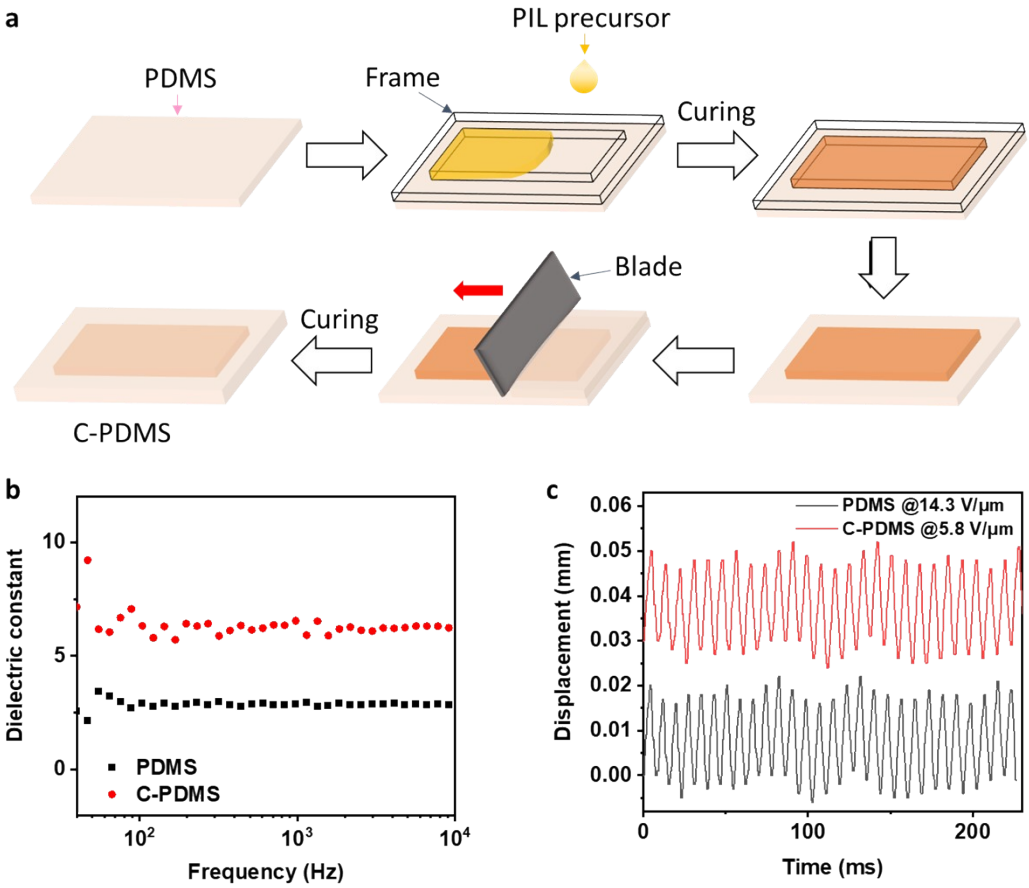

Fig. S16. (a) Schematic of the fabrication of C-PDMS. (b) Dielectric constant of PDMS and C-PDMS. (c) Cyclic actuation of bending DEAs with PDMS at 14.3 V/μm and with C-PDMS at 5.8 V/μm and 100 Hz.

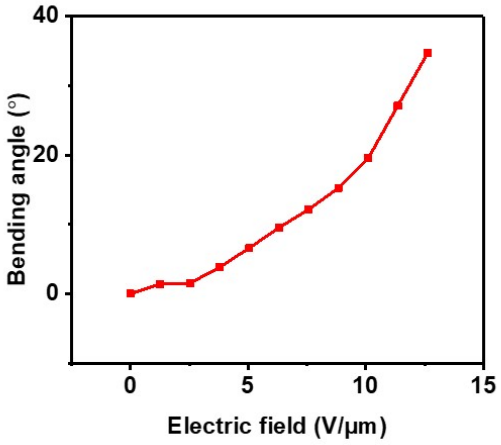

Fig. S17. Bending angles of the integrated bending DEA and ACEL, where ACEL functions as a passive layer.

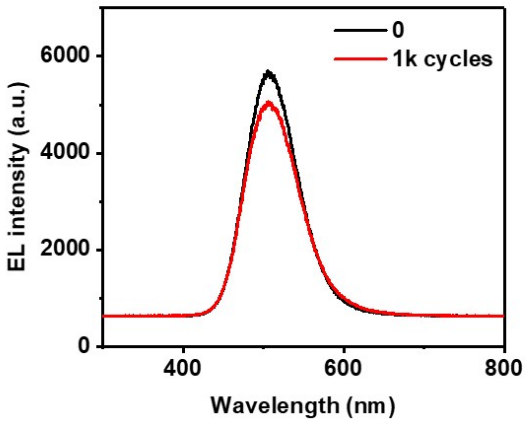

Fig. S18. The emission spectrum of the light emissive bending DEA at initial state and after 1000 cycles of bending.

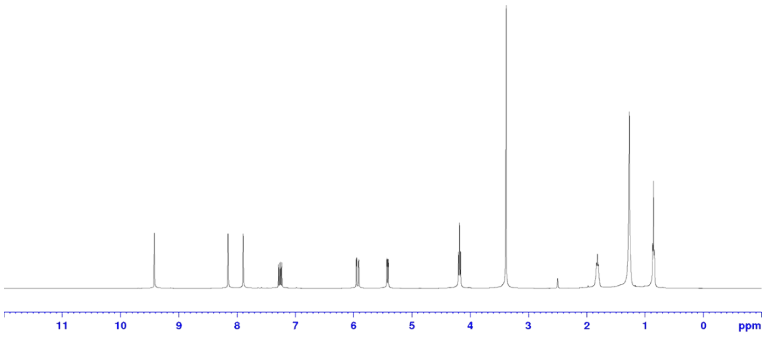

Fig. S19. ^{1}H NMR spectra of HVIM BF_4 in DMSO-d_6.

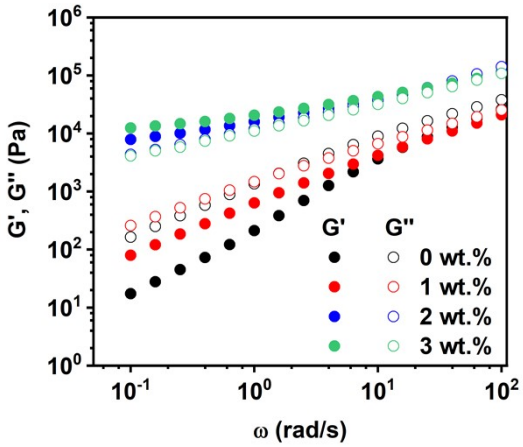

Fig. S20. Frequency-dependent storage modulus (G') and loss modulus (G") of PILs with different weight percentage of PEGDA 700. The solvent amount is fixed at 100 wt.%.

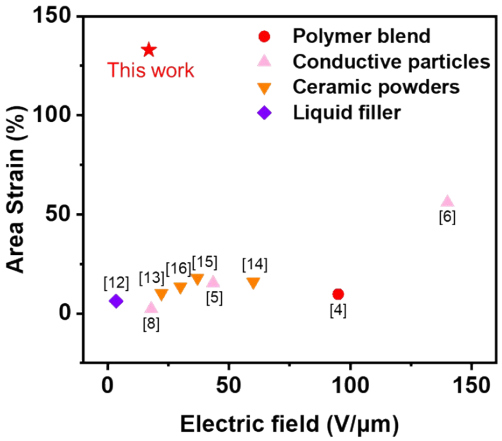

Fig. S21. Ashby plot of area strains vs electric fields of DEAs with different kinds of fillers.

Table S1. Properties of PILs with different solvent amount in precursors.

Sample	Liquid/solid	Swelling ratio	T_g (°C)	Strain at break (%)	Young's modulus (MPa)	Adhesion property
PIL-0	Solid	3.41±0.47	174.8	14.0±8.8	125.9±13.8	Not adhesive
PIL-50	Solid	6.61±0.59	78.3	163.2±53.4	15.3±5.3	Slightly adhesive
PIL-100	Solid	9.11±1.41	-52.1	276.4±21.3	0.11±0.03	Strongly adhesive
PIL-150	Liquid	N.A.	-55.5	N.A.	N.A.	N.A.

Table S2. Comparison of dielectric constant and actuation performance of this work against other DEAs with fillers.

Elastomer matrix	Filler type	Filler	Filler loading	Dielectric constant (1 kHz)	Young's modulus (MPa)	Actuated area	Electrical field (V/μm)	Ref.
VHB	polymer	PIL	200 μL (precursor)	13.4	0.21	133%	17	This work
SEBS		PU	10 wt%	4	2.1	9.8%	95	[4]
PDMS	Conductive particles	poly(divinylbenzene) – encapsulated polyaniline	20 wt%	~3.5	2.324	15.5% (lateral)	43.5	[5]
Acrylate copolymer		Al nanoparticles	4.0 vol%	8.4	0.53	56%	140	[6]
PU		CNT:graphene	1:2 (sum 2.5 wt%)	~170	14.47	72.5% (thickness strain)	35.4	[7]
carboxylated nitrile butadiene rubber (XNBR)		Graphene:poly (dopamine) (PDA)	1:2 (sum 0.5 phr)	~10	3.63	2.4%	18	[8]
Vinyl-terminated PDMS	liquid	1-butyl-3-methylimidazolium hexafluoroantimonate ($BmimSbF_6$)	90 phr	~7.6	0.15	N.A.	7.5 (breakdown strength)	[9]
PDMS [sylgard 184]		glycerol	120 phr	~16	0.33	N.A.	N.A.	[10]
PDMS [sylgard 184]		EGaIn (liquid metal)	20 vol%	~8	~2	N.A.	N.A.	[11]
PDMS [sylgard 184]		EMIM TFSI	20 vol%	~7	0.01	6.27%	~3.5 (8 kV)	[12]
polymethylvinylsiloxane (PMVS)	Ceramic powders	epoxy-functionalized TiO_2	20 phr	7.50	0.15	10.2%	22.2	[13]
acrylonitrile butadiene rubber [NBR]		poly(dopamine) and silane surfacefunctionalized TiO_2 nanoparticles	20 phr	~15.75	~1.475	16%	60	[14]
hydrogenated nitrile-butadiene rubber (HNBR)		TiO_2 ESO	10 wt% 30 wt%	~11.5	0.6	13.6%	30	[15]
PDMS		TiO_2 DMSO	3.6 vol% 100 phr	3.5	0.095	~18%	~37	[16]

References

1 E. Hajiesmaili and D. R. Clarke, *J. Appl. Phys.*, 2021, **129**, 151102.

2 M. W. M. Tan, H. Bark, G. Thangavel, X. Gong and P. S. Lee, *Nat. Commun.*, 2022, **13**, 6769.

3 M. Duduta, E. Hajiesmaili, H. Zhao, R. J. Wood and D. R. Clarke, *Proceedings of the National Academy of Sciences of the United States of America*, 2019, **116**, 2476-2481.

4 H. Aguilar Bolados, M. Hernández-Santana, L. J. Romasanta, M. Yazdani-Pedram, R. Quijada, M. A. López-Manchado and R. Verdejo, *Polymer*, 2019, **171**, 25-33.

5 D. M. Opris, M. Molberg, C. Walder, Y. S. Ko, B. Fischer and F. A. Nüesch, *Adv. Funct. Mater.*, 2011, **21**, 3531-3539.

6 W. Hu, S. N. Zhang, X. Niu, C. Liu and Q. Pei, *J. Mater. Chem. C*, 2014, **2**, 1658.

7 T. Chen, L. Pan, M. Lin, B. Wang, L. Liu, Y. Li, J. Qiu and K. Zhu, *Polym. Test.*, 2015, **47**, 4-11.

8 D. Yang, X. Kong, Y. Ni, M. Ruan, S. Huang, P. Shao, W. Guo and L. Zhang, *Polymers*, 2019, **11**.

9 X. Liu, L. Yu, Y. Nie and A. L. Skov, *Adv. Eng. Mater.*, 2019, **21**, 1900481.

10 P. Mazurek, L. Yu, R. Gerhard, W. Wirges and A. L. Skov, *J. Appl. Polym. Sci.*, 2016, **133**, 44153.

11 C. Pan, E. J. Markvicka, M. H. Malakooti, J. Yan, L. Hu, K. Matyjaszewski and C. Majidi, *Adv. Mater.*, 2019, **31**, e1900663.

12 Ankit, N. Tiwari, F. Ho, F. Krisnadi, M. R. Kulkarni, L. L. Nguyen, S. J. A. Koh and N. Mathews, *ACS Appl. Mater. Interfaces*, 2020, **12**, 37561-37570.

13 X. Liu, H. Sun, S. Liu, Y. Jiang, B. Yu, N. Ning, M. Tian and L. Zhang, *Chem. Eng. J.*, 2020, **393**, 124791.

14 D. Yang, M. Ruan, S. Huang, Y. Wu, S. Li, H. Wang, Y. Shang, B. Li, W. Guo and L. Zhang, *J. Mater. Chem. C*, 2016, **4**, 7724-7734.

15 D. Yang, L. Zhang, N. Ning, D. Li, Z. Wang, T. Nishi, K. Ito and M. Tian, *RSC Adv.*, 2013, **3**, 21896.

16 H. Zhao, D.-R. Wang, J.-W. Zha, J. Zhao and Z.-M. Dang, *J. Mater. Chem. A*, 2013, **1**, 3140.